POPULATION DYNAMICS

Boom-bust cycles in gray whales associated with dynamic and changing Arctic conditions

Joshua D. Stewart[1]*, Trevor W. Joyce[2,3], John W. Durban[3,4], John Calambokidis[5], Deborah Fauquier[6], Holly Fearnbach[4], Jacqueline M. Grebmeier[7], Morgan Lynn[3], Manfredi Manizza[8], Wayne L. Perryman[3], M. Tim Tinker[9,10], David W. Weller[3]

Climate change is affecting a wide range of global systems, with polar ecosystems experiencing the most rapid change. Although climate impacts affect lower-trophic-level and short-lived species most directly, it is less clear how long-lived and mobile species will respond to rapid polar warming because they may have the short-term ability to accommodate ecological disruptions while adapting to new conditions. We found that the population dynamics of an iconic and highly mobile polar-associated species are tightly coupled to Arctic prey availability and access to feeding areas. When low prey biomass coincided with high ice cover, gray whales experienced major mortality events, each reducing the population by 15 to 25%. This suggests that even mobile, long-lived species are sensitive to dynamic and changing conditions as the Arctic warms.

The Bering and Chukchi seas in the Pacific Arctic are extremely productive shallow basins (*1*–*3*) that support seasonal foraging opportunities for a wide variety of migratory and Arctic-associated taxa (*4*). The Pacific Arctic food web is characterized by ice-associated algal growth during spring and early summer, which is transported to the benthos through decay and sinking of particulate organic carbon (*3*). This tight pelagic-benthic coupling historically resulted in some of the most productive nearshore benthic systems in the world (*3*), attracting migrants from throughout the Pacific and supporting large populations of marine species (*4*, *5*).

As the Arctic has rapidly warmed, sea ice retreat has occurred progressively earlier in the spring, and the Bering and Chukchi seas have remained ice free for longer in the autumn (*6*). This has resulted in increased water-column productivity (*7*, *8*) but has reduced the amount of particulate organic carbon that reaches the sea floor through pelagic-benthic coupling that is dependent on sinking ice-associated algae (*5*). In addition, decreased sea ice cover allows stronger current-driven flow over the shallow basins of the Pacific Arctic, reducing the quantity of finer-sediment grain size within the benthos that support habitat for tube-building amphipods, which have some of the highest lipid content of benthic crustaceans (*9*, *10*). Collectively, these impacts have driven changes to the structure of Arctic benthic communities, which may translate into impacts on higher-trophic-level species that migrate seasonally to access these foraging hotspots (*5*, *9*, *10*).

Eastern North Pacific gray whales (*Eschrichtius robustus*) undertake one of the longest mammalian migrations between wintering areas in Baja California, Mexico, and summer feeding areas in the Bering and Chukchi seas to take advantage of these highly concentrated benthic prey resources (*11*). Gray whales have specialized baleen plates adapted to suction feeding in soft sediments and are the only baleen whale to feed primarily on benthic prey (*11*). Although they are capable of feeding on pelagic zooplankton, the diet of gray whales feeding in the Arctic is dominated by benthic crustaceans—in particular, ampeliscid amphipods—that are found in abundance in shallow Arctic basins (*12*).

Estimates of pre-whaling population sizes range from 15,000 to 30,000 individuals for the eastern North Pacific gray whale population, based on population models fitted to estimates from abundance surveys combined with commercial and aboriginal harvest data (*13*). Genetic estimates of prehistoric abundance are much higher, ranging from ~75,000 to 120,000 individuals (*14*), although this likely included the now endangered western North Pacific population and may reflect a larger carrying capacity supported by increased benthic habitat availability during the Last Glacial Minimum (*15*). Commercial whaling in the lagoons of Baja California and throughout the North Pacific depleted the eastern North Pacific gray whale population to fewer than 5000 individuals by the early 1900s (*13*). A rapid and sustained post-whaling increase in abundance led to the delisting of the population from the Endangered Species Act in 1[illegible] and is widely viewed as an iconic example of successful conservation and species recovery (*16*).

The status and stability of eastern North Pacific gray whales has come into question as the population experienced two major documented mortality events in 1999–2000 and 2019–2022 (*17*, *18*). In response to the first mortality event in 1999, there was speculation that the population may have reached its carrying capacity and was suffering from density-dependent effects on survival (*19*). In light of fluctuations in reproductive output and a second major mortality event two decades later, many studies have proposed that variable and changing Arctic conditions may be drivers of eastern North Pacific gray whale population dynamics (*12*, *20*–*22*).

Arctic sea ice extent has been proposed as a contributor to gray whale vital rates—especially reproduction—by physically restricting access to summer feeding areas (*20*, *22*, *23*). However, in recent years previously identified relationships between gray whale reproduction and Arctic sea ice extent have begun to decouple (*22*, *23*), and variability in sea ice has been insufficient to explain mortality rates (*20*). Eastern North Pacific gray whales have the most complete long-term abundance and demographic data available for any large whale species, and we leveraged these extensive datasets to examine environmental drivers of population dynamics not possible in other species. We combined time series of gray whale abundance, reproduction, nutritive condition, and strandings spanning more than half a century into a population dynamics model to estimate annual carrying capacity for the population. We show that this annual carrying capacity is well explained by ice-mediated access to the population's primary foraging grounds in the Arctic and biomass of benthic crustaceans. The observed boom-bust cycles in gray whale abundance and vital rates suggest that as large whales recover from post-whaling depletion, their populations may become increasingly governed by environmental constraints and climate variability.

Results and discussion

We combined 31 estimates of eastern North Pacific gray whale abundance over 54 years (1968 to 2022) (*24*), 30 estimates of calf production over 42 years (1980 to 2022) (*22*, *25*), 1391 records of stranded gray whales on the United States coastline over 48 years (1974 to 2022), and 1334 body condition measurements over 32 years (1987 to 2019) (*26*) into an integrated population dynamics model that estimates annual abundance, birth rates, and mortality rates. The model uses evidence of human interactions in stranded gray whales to estimate proportional hazards of anthropogenic and natural contributions to mortality.

[1]Ocean Ecology Lab, Marine Mammal Institute, Department of Fisheries, Wildlife and Conservation Sciences, Oregon State University, Newport, OR, USA. [2]Ocean Associates, Arlington, VA, USA. [3]Marine Mammal and Turtle Division, National Oceanic and Atmospheric Administration (NOAA) Southwest Fisheries Science Center, La Jolla, CA, USA. [4]Sealife Response, Rehabilitation and Research (SR3), Des Moines, WA, USA. [5]Cascadia Research Collective, Olympia, WA, USA. [6]Office of Protected Resources, National Marine Fisheries Service, Silver Spring, MD, USA. [7]Chesapeake Biological Laboratory, University of Maryland Center for Environmental Science, Solomons, MD, USA. [8]Geosciences Research Division, Scripps Institution of Oceanography, University of California San Diego, La Jolla, CA, USA. [9]Nhydra Consulting, Halifax, NS, Canada. [10]Ecology and Evolutionary Biology, University of California, Santa Cruz, Santa Cruz, CA, USA.
*Corresponding author. Email: joshua.stewart@oregonstate.edu

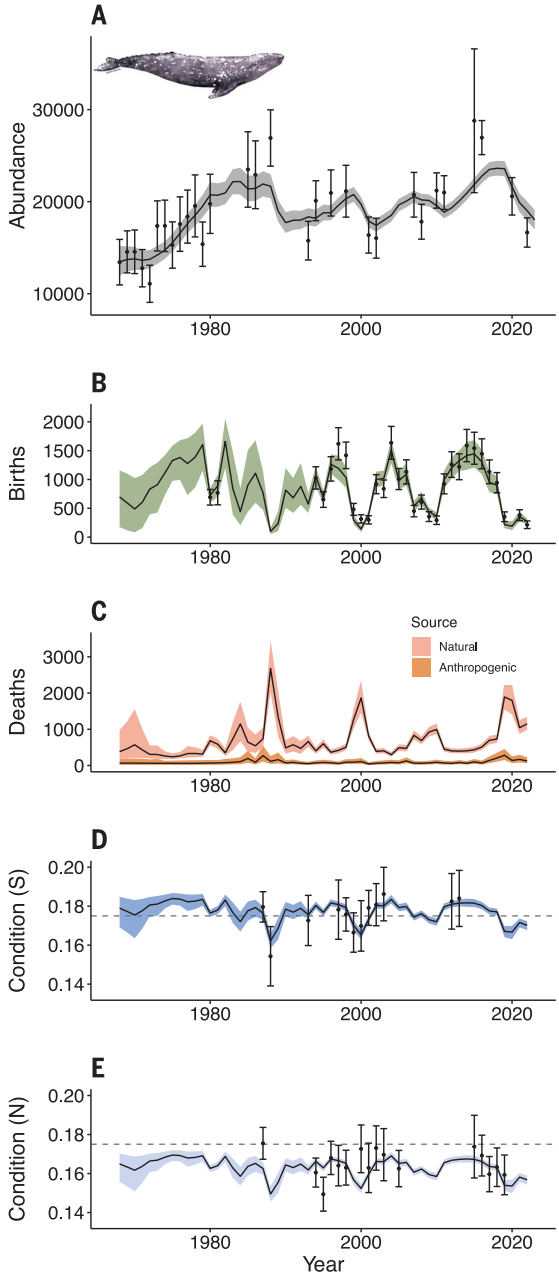

Fig. 1. Population dynamics of eastern North Pacific gray whales. (**A**) Gray whales have experienced major fluctuations in abundance after an initial post-whaling recovery, including three major declines beginning in 1987, 1999, and 2019. (**B** to **E**) These declines and subsequent recoveries in the 1990s and 2000s were associated with synchronous changes in (B) births and (C) mortality, as well as changes in nutritive condition in (D) southbound and (E) northbound migrating whales. Black points in (A) and (B) indicate the median estimated abundance and calf production from visual surveys, with standard errors of model estimates (vertical bars). Black points in (D) and (E) indicate the mean values of body condition measurements from each survey year and the standard deviation of observations (vertical bars). In (A) to (E), the black lines indicate the median of the posterior distribution of model-estimated values, and the shaded regions indicate the 95% posterior credible intervals.

In addition, the model estimates both the long-term carrying capacity (K), as well as an annually varying carrying capacity (K_t) that reflects year-to-year variation in the strength of negative density dependence as determined by environmental covariates and stochastic effects. We considered three Arctic time series as candidate covariates for annual gray whale carrying capacity: (i) access to feeding grounds, defined as the number of days with <50% sea ice cover on the historic gray whale foraging grounds in the Chirikov basin and southern Chukchi Sea (1979 to 2021) (*23*, *27*); (ii) benthic infaunal crustacean biomass, averaged over the same foraging hotspots as sea ice access (1971 to 2019) (*28*); and (iii) zooplankton density estimated by using a global ocean ecosystem model that includes the entire Arctic Ocean ecosystem, averaged over gray whale foraging hotspots (1992 to 2020) (*29*). The data and population model are described in detail in the Data sources and Integrated population model sections of the supplementary materials.

The eastern North Pacific gray whale population has experienced three major mortality events, each resulting in reductions of 15 to 25% of total abundance within the half-century of nearly continuous monitoring, representing extraordinarily high periodic mortality rates for a long-lived vertebrate (Fig. 1). These mortality events were associated with peaks in reported strandings during the 1999–2000 and 2019–2022 periods. The 1987–1989 abundance decline is the largest in magnitude but was not associated with an increase in strandings, likely because reporting structures and survey effort to detect strandings were expanded and improved substantially beginning in 1990. However, this major impact to the population is also reflected in the poorest recorded body condition of the survey history in 1988, falling rapidly from very good condition in 1987 (Fig. 1D). The population dynamics model estimated low annual carrying capacities (K_t) of approximately 10,000 individuals during each of these die-offs (Fig. 2A), indicating that Arctic foraging grounds periodically experience major disruptions, limiting the number of whales that they can support. These fluctuations in annual carrying capacity were represented in mortality rates, body condition, and most strongly in birth rates, which had the greatest proportional change with varying carrying capacity (fig. S5). On the basis of anthropogenic injury rates in stranded whales, model-estimated anthropogenic mortality rates remained low and stable, whereas natural mortality rates varied substantially and peaked during major die-offs, suggesting direct human impacts such as vessel strikes and entanglements in fishing gear are not the primary drivers of mortality in this population.

The maximum birth rate estimated by the model was 0.111 (95% credible intervals 0.108 to 0.114). The realized annual birth rate ranged from a low of 0.0046 in 1998 (0.0024 to 0.0076) to a high of 0.085 in 1975 (0.062 to 0.102). Within the span of calf production observations (1994–2022), the minimum birth rate was 0.007 in 2000 (0.004 to 0.01), and the maximum was 0.082 in 2004 (0.069 to 0.09). The minimum estimated mortality rate was 0.011 (0.009 to 0.014). The realized annual mortality rate ranged from a low of 0.019 in 1975 (0.014 to 0.027) to a high of 0.13 in 1988 (0.099 to 0.162). During the three major mortality events, median estimated mortality rates were 0.13 and 0.079 (in 1988 and 1989); 0.065 and 0.099 (in 1999 and 2000); and 0.092, 0.089, 0.061, and 0.067 (from 2019 to 2022).

Model-estimated mean body condition was lowest in 1988 [median 0.162, 95% confidence interval (CI) 0.158 to 0.166], 2000 (0.165, 0.163 to 0.168), and 2020 (0.167, 0.163 to 0.170). The highest estimated body condition was in 1975 (0.184, 0.181 to 0.187), although there were no photogrammetric measurements before 1987. The 3 years with highest estimated body condition and corresponding condition measurements were 2013 (0.181, 0.180 to 0.183), 2012 (0.181, 0.179 to 0.183), and 1997 (0.181, 0.179 to 0.182). The estimated northbound body

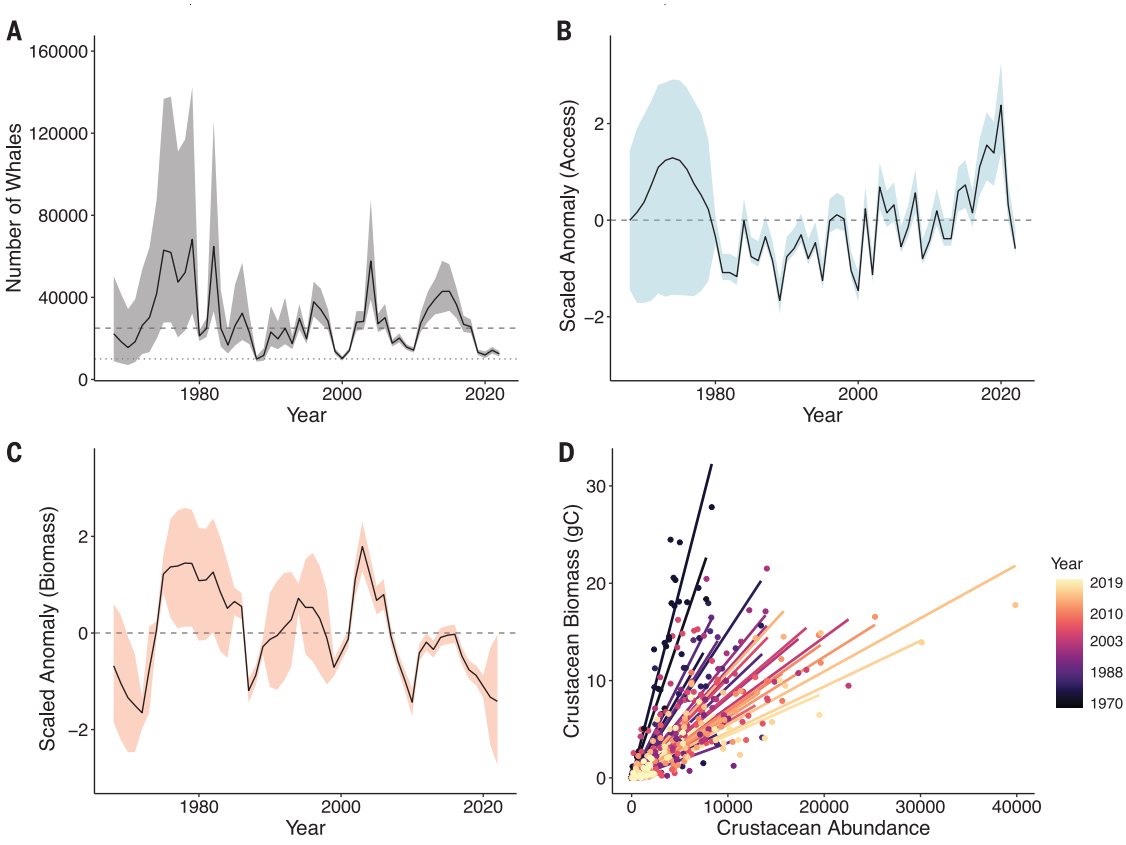

Fig. 2. Drivers of eastern North Pacific gray whale carrying capacity. (**A**) Estimated annual carrying capacity (K_t) from the population dynamics model, with reference lines at 25,000 (dashed line) and 10,000 (dotted line). (**B**) Estimated ice access anomaly, which is the *Z*-scored number of days with 50% or lower ice cover on gray whale feeding grounds. (**C**) Estimated crustacean biomass anomaly, which is the *Z*-scored mean grams of carbon of benthic crustaceans on key gray whale feeding grounds. (**D**) Decline in benthic crustacean per capita biomass from 1970 to 2019, showing the relationship each sampling year between benthic crustacean abundance and biomass in grams of carbon (gC). In (A) to (C), the black lines indicate the median of the posterior distribution of estimates, and the shaded regions indicate the 95% posterior credible intervals.

condition scaling factor was 0.922 (0.913 to 0.930), indicating an ~8% decline in body condition between southbound and northbound measurements.

The estimated long-term average K was 22,062 (18,967 to 24,725). This long-term average is lower than the median of annual K_t values (24,500, 95% CI 21,771 to 27,797), which is to be expected given that it is the arithmetic mean outcome of a stochastic process and thus reflects the effects of environmental variability on expected abundance (*30*).

We found a significant positive relationship between benthic crustacean biomass and carrying capacity (99.9% probability slope > 0), no relationship with zooplankton density (39.2% > 0), and a high probability of a positive relationship with sea ice access (93.5% > 0). With the zooplankton density covariate eliminated from the model, both crustacean biomass (100% > 0) and sea ice access (96.2% > 0) had significant positive relationships with carrying capacity. This suggests that the ability of the eastern North Pacific gray whale population to physically access key feeding areas, in combination with in situ prey availability, explains fluctuations in body condition, reproduction, and mortality. The three major mortality events occurred during periods of simultaneous low crustacean biomass and restricted access to feeding areas (Fig. 2). In 2010, a rapid decrease in crustacean biomass but a period of average ice access led to a depression in birth rates and a modest decrease in abundance but not a major mortality event. The onset of the 2019 mortality event appears to have been driven initially by low crustacean biomass and exacerbated by a steep reduction in access to feeding areas over the following 2 years.

The decision to model gray whale population dynamics by applying annual covariate effects to carrying capacity (K), rather than the population's intrinsic growth rate (r), is uncommon. Although in theory either model formulation could be used to explain fluctuations in abundance and vital rates, we believe that applying covariate effects to carrying capacity better reflects biological reality. The Bering and Chukchi seas are the primary feeding area for virtually all eastern North Pacific gray whales, suggesting that the quality and quantity of prey in these areas will have a greater impact on vital rates when there is high intraspecific competition at higher levels of gray whale abundance. This is supported empirically by our estimates of population growth rate relative to abundance. Mean population growth rates were significantly higher at low than at high abundance levels, and major busts (annual declines of >9 to 10%) only occurred when the gray whale population was at high abundance (fig. S9), which supports the existence of density-dependent controls on vital rates. By applying covariate effects to carrying capacity, we simultaneously account for environmental conditions and the effects of negative density dependence (*31*). In addition, this avoids a scenario in which, in a model that applies covariate effects to r instead of K, the population exceeds a stationary carrying capacity but continues to grow because of positive covariate effects on growth rate. Instead, our estimated annual carrying capacity (K_t) captures short-term fluctuations in the strength of density dependence and can be interpreted as an abstract parameter corresponding to the expected equilibrium abundance if environmental conditions remained fixed at the values recorded during that year (*32*).

Over the past 50 years, the per capita biomass of benthic infaunal crustaceans has declined precipitously (Fig. 2D and fig. S3), and the three major gray whale mortality events coincided with periods of low per capita biomass, which translated into low total crustacean biomass. This decline in per capita biomass is most likely associated with species distribution shifts of benthic amphipods and other

crustaceans. As ice cover decreases in response to rapid Arctic warming, current speed in the Chirikov basin has increased, leading to larger sediment grain size and reduced particulate organic carbon reaching the seafloor (*5*). These conditions favor smaller amphipods with lower lipid content over the lipid-rich, tube-building ampeliscid amphipods that historically dominated the shallow basins of the Bering and Chukchi seas (*10*). This regime shift has likely contributed to declining per capita biomass of gray whale prey, which despite steady or increasing prey abundance has resulted in lower overall available biomass (fig. S3).

The combined effect of sea ice cover and benthic productivity on gray whale population dynamics has driven major boom-bust cycles, including two modern booms in abundance that may have exceeded preexploitation levels (*13*). High benthic biomass and prey quality in the late 1970s and early 1980s supported almost 25,000 gray whales, contributing to their delisting from the US Endangered Species Act. More recently, rapid Arctic warming in response to climate change increased access to feeding areas (Fig. 2B), supporting a sustained increase in gray whale abundance over the past decade (Fig. 1A). Although recent Arctic warming may have provided sufficient benefit to the population to counteract decreasing benthic biomass over the short term, the outlook for benthic prey quality is not favorable. Rising water column and bottom water temperatures and projected decoupling of pelagic and benthic productivity caused by retreating sea ice will likely lead to continued declines in Arctic benthic crustacean biomass (*5*). Access to feeding areas reached a peak of 266 days in 2019, which is presumably approaching a point of diminishing returns given that the species migrates to Mexico each winter. Poleward shifts in gray whale feeding locations have already been documented, which likely reflect the declining quality and shifting distribution of their preferred prey (*12*). Future declines in benthic biomass will likely drive decreases in gray whale carrying capacity that cannot be offset by continued increases in ice access. Reports of gray whales shifting their Arctic feeding distribution and targeting pelagic prey (*12*) suggest that they may have the ability to compensate for these changing conditions to some extent, but our results suggest that any ongoing behavioral adaptations have thus far been insufficient to prevent major mortality events.

Eastern North Pacific gray whales are the most closely monitored large whale species, with records of abundance, reproduction, mortality, and condition spanning more than half a century. The abundance of most large whale species remains far below pre-whaling levels (*33*, *34*), which limits our understanding of the dynamics and behavior of whale populations as they approach carrying capacity and become increasingly governed by density-dependent processes. By contrast, gray whales have recovered rapidly from post-whaling lows to numbers that may approach or exceed pre-whaling levels and have low rates of direct human mortality, providing a rare window into the possible natural fluctuations of large whale populations. The periodic mortality events and major population swings that we report are surprising for a long-lived vertebrate that must by definition have high average survival rates to facilitate longevity. However, whales achieve their immense body sizes by feeding on large quantities of low-trophic-level prey (*35*), which may make them sensitive to oceanographic and environmental fluctuations. The feeding-fasting cycles associated with migratory baleen whales may also increase their susceptibility to environmental perturbations. Gray whales migrate more than 15,000 km each year and rely on a 4- to 5-month feeding season to support a majority of their energetic requirements for the year. This strategy may place them at a physiological threshold at which disruptions to their food supply translate into major impacts to vital rates—a pattern that may be widespread across migratory whales and may become more pronounced as species and populations recover to their pre-whaling abundances. Climate-driven ocean warming is expected to have profound impacts on ocean circulation, upwelling strength, and primary production (*36*, *37*), which may in turn have major implications for large whale population dynamics and viability through predator-prey interactions (*34*).

REFERENCES AND NOTES

1. R. C. Highsmith, K. O. Coyle, *Nature* **344**, 862–864 (1990).
2. A. M. Springer, C. P. McRoy, M. Flint, *Fish. Oceanogr.* **5**, 205–223 (1996).
3. J. M. Grebmeier, L. W. Cooper, H. M. Feder, B. I. Sirenko, *Prog. Oceanogr.* **71**, 331–361 (2006).
4. K. J. Kuletz *et al*., *Prog. Oceanogr.* **136**, 175–200 (2015).
5. J. M. Grebmeier *et al*., *Science* **311**, 1461–1464 (2006).
6. H. P. Huntington *et al*., *Nat. Clim. Chang.* **10**, 342–348 (2020).
7. K. R. Arrigo, G. L. van Dijken, *Prog. Oceanogr.* **136**, 60–70 (2015).
8. K. M. Lewis, G. L. van Dijken, K. R. Arrigo, *Science* **369**, 198–202 (2020).
9. J. M. Grebmeier, K. E. Frey, L. W. Cooper, M. Kędra, *Oceanography* **31**, 136–151 (2018).
10. J. M. Grebmeier, S. E. Moore, J. E. Overland, K. E. Frey, R. Gradinger, *Eos* **91**, 161–162 (2010).
11. G. C. Pike, *J. Fish. Res. Board Can.* **19**, 815–838 (1962).
12. S. E. Moore *et al*., *PLOS ONE* **17**, e0265934 (2022).
13. A. E. Punt, C. Allison, G. Fay, *J. Cetacean Res. Manag.* **6**, 121–132 (2004).
14. S. E. Alter, E. Rynes, S. R. Palumbi, *Proc. Natl. Acad. Sci. U.S.A.* **104**, 15162–15167 (2007).
15. N. D. Pyenson, D. R. Lindberg, *PLOS ONE* **6**, e21295 (2011).
16. P. J. Clapham, S. B. Young, R. L. Brownell, *Mammal Rev.* **29**, 37–62 (1999).
17. B. J. Le Boeuf, H. Pérez-Cortés M., J. Urbán R., B. R. Mate, F. Ollervides U., *J. Cetacean Res. Manag.* **2**, 85–99 (2000).
18. F. Christiansen *et al*., *Mar. Ecol. Prog. Ser.* **658**, 237–252 (2020).
19. S. E. Moore *et al*., *Mar. Mamm. Sci.* **17**, 954–958 (2001).
20. J. R. Brandon, A. E. Punt, "Assessment of the eastern stock of North Pacific gray whales: incorporating calf production, sea-ice and strandings data," paper SC/61/AWMP2 presented to the International Whaling Commission (IWC) Scientific Committee (2009).
21. A. E. Punt, P. R. Wade, "Population status of the eastern North Pacific stock of gray whales in 2009," US Department of Commerce, National Oceanic and Atmospheric Administration (NOAA) Technical Memo NMFS-AFSC-207, 43 (2009).
22. W. L. Perryman, T. Joyce, D. W. Weller, J. W. Durban, *Mar. Mamm. Sci.* **37**, 448–462 (2020).
23. T. W. Joyce *et al*., *Mar. Ecol. Prog. Ser.* **709**, 141–158 (2023).
24. T. Eguchi, A. R. Lang, D. W. Weller, "Abundance and migratory phenology of Eastern North Pacific gray whales 2021/2022," US Department of Commerce, NOAA Technical Memorandum NMFS-SWFSC-668 (2022).
25. T. Eguchi, A. R. Lang, D. W. Weller, "Eastern North Pacific gray whale calf production 1994-2022," US Department of Commerce, NOAA Technical Memorandum NMFS-SWFSC-667 (2022).
26. W. L. Perryman, M. S. Lynn, *J. Cetacean Res. Manag.* **4**, 155–164 (2002).
27. G. Gailey *et al*., *Sci. Rep.* **10**, 1553 (2020).
28. J. M. Grebmeier, L. W. Cooper, Benthic macroinfaunal and dominant taxa samples collected from Northern Bering Sea to Chukchi Sea, 1970–2019 (2023); https://arcticdata.io/catalog/view/doi%3A10.18739%2FA24T6F480.
29. D. Carroll *et al*., *J. Adv. Model. Earth Syst.* **12**, e2019MS001888 (2020).
30. R. C. Lewontin, D. Cohen, *Proc. Natl. Acad. Sci. U.S.A.* **62**, 1056–1060 (1969).
31. J. Roughgarden, *Am. Nat.* **109**, 713–736 (1975).
32. D. G. Heckel, J. Roughgarden, *Proc. Natl. Acad. Sci. U.S.A.* **77**, 7497–7500 (1980).
33. C. Scott Baker, P. J. Clapham, *Trends Ecol. Evol.* **19**, 365–371 (2004).
34. V. J. D. Tulloch, É. E. Plagányi, C. Brown, A. J. Richardson, R. Matear, *Glob. Change Biol.* **25**, 1263–1281 (2019).
35. M. S. Savoca *et al*., *Nature* **599**, 85–90 (2021).
36. O. Hoegh-Guldberg, J. F. Bruno, *Science* **328**, 1523–1528 (2010).
37. G. C. Hays, A. J. Richardson, C. Robinson, *Trends Ecol. Evol.* **20**, 337–344 (2005).
38. J. D. Stewart *et al*., stewart6/ENPGW-IPM: Data and Code for Stewart *et al*. Boom-bust cycles in gray whales. Zenodo (2023); https://doi.org/10.5281/zenodo.8201214.

ACKNOWLEDGMENTS

We thank past and present members of the Working Group for Marine Mammal Unusual Mortality Events; the Gray Whale Unusual Mortality Event Investigative Teams; as well as the US, Canadian, and Mexico marine mammal stranding network responders. We thank the NOAA Office of Marine and Aviation Operations and D. LeRoi for their support of drone flights to measure whale body condition. We thank J. Baker for feedback on analyses and interpretation. The scientific results and conclusions and any views or opinions expressed herein are those of the authors and do not necessarily reflect the views or policies of the US government, its agencies, or any of the included organizations. **Funding:** J.D.S. was supported by a National Academies NRC Research Associateship and the Oregon State University Marine Mammal Institute Research Endowment. Abundance, calf production, and aerial photogrammetry surveys were supported by NOAA, US Department of Commerce. Drone photogrammetry surveys at Piedras Blancas, California, from 2015 to 2019 were supported by SeaLife Response, Rehabilitation, and Research (SR3) and NOAA, with facility and property use provided by the Bureau of Land Management, US Department of the Interior. J.M.G. was supported for benthic time series sampling for crustaceans and associated fauna through multiple awards, most recently the US National Science Foundation Office of Polar Programs

(OPP 1917469) and the National Oceanic and Atmospheric Administration Arctic Research Program (CINAR 25984.02).
Author contributions: Conceptualization: J.D.S. and J.W.D. Funding acquisition: W.L.P., J.W.D., D.W.W., and H.F. Investigation: All authors. Methodology: J.D.S., J.W.D., W.L.P., D.W.W., and M.T.T.; Data curation: T.W.J., J.W.D., J.C., D.F., H.F., J.M.G., M.L., M.M., W.L.P., and D.W.W. Formal analysis: J.D.S. and M.T.T. Visualization: J.D.S. Writing – original draft: J.D.S. Writing – review and editing: All authors. **Competing interests:** The authors declare no competing interests. **Data and materials availability:** All data and code required to reproduce the analyses presented in the main text and online supplementary materials are available online through Zenodo (*38*). **License information:**

SUPPLEMENTARY MATERIALS

science.org/doi/10.1126/science.adi1847
Materials and Methods
Figs. S1 to S9
References (*39*–*55*)
MDAR Reproducibility Checklist

Submitted 8 April 2023; accepted 16 August 2023
10.1126/science.adi1847

Boom-bust cycles in gray whales associated with dynamic and changing Arctic conditions

Joshua D. Stewart, Trevor W. Joyce, John W. Durban, John Calambokidis, Deborah Fauquier, Holly Fearnbach, Jacqueline M. Grebmeier, Morgan Lynn, Manfredi Manizza, Wayne L. Perryman, M. Tim Tinker, and David W. Weller

Science **382** (6667), . DOI: 10.1126/science.adi1847

Editor's summary

Environments are responding to human-induced climate warming in a variety of ways, not all of them expected. Such changes can have large impacts on species and ecosystems. Responses to such changes may be most obvious in shorter-lived species, but Stewart *et al*. show that even some of the largest animals on the planet are susceptible to relatively minor changes (see the Perspective by Read). Specifically, they looked across a 50-year database on gray whale population estimates and found clear evidence of rapid population increases and declines in response to changing prey biomass and ice cover. —Sacha Vignieri

Science
AAAS

Supplementary Materials for

Boom-bust cycles in gray whales associated with dynamic and changing Arctic conditions

Joshua D. Stewart *et al*.

Corresponding author: Joshua D. Stewart, joshua.stewart@oregonstate.edu

Science **382**, 207 (2023)
DOI: 10.1126/science.adi1847

The PDF file includes:

Other Supplementary Material for this manuscript includes the following:

Materials and Methods

Data Sources

Eastern North Pacific gray whales migrate annually from their productive summer feeding grounds in the Arctic to overwintering lagoons on the Baja California peninsula, Mexico, where reproduction occurs and females give birth to calves. For the purposes of our analyses, we assume that the entire population undertakes the annual migration between the Arctic and Mexico each year, although there is a known subpopulation of whales that feed along the Pacific coast of the U.S. and Canada in the summer months, and a number of observations of gray whales outside of their expected seasonal range that challenge this assumption. However, compared to the scale of the entire eastern North Pacific population (~25,000 whales), these subpopulation dynamics (e.g. ~350 whales in the Pacific Coast Feeding Group) most likely do not make a meaningful impact on our model inferences. While the annual migration crosses three countries, most of the survey effort is concentrated in California and along the U.S. west coast as we describe below.

Abundance

The longest-running time series in our analysis is of abundance estimates, generated from counts of southbound gray whales migrating along the U.S. west coast from 1967 – 2022 (*24*, *39*, *40*). Surveys take place from early December to late February at Granite Canyon, in central California, and we consider the index year to be from the January of each survey (i.e. an abundance estimate generated from the December 2019 – February 2020 survey would be considered the 2020 estimate). Southbound migrants are presumed to be adults and juveniles. While females occasionally give birth to calves before reaching Baja California, this is rare and new calves would make a negligible contribution to southbound migration abundance estimates. Counts were not undertaken every year during this period, and the method used to estimate abundance changed in 2006. Abundance estimation from 1967 – 2006 is described in (*41*) whereas the method used from 2006 – 2022 is described in (*40*). We note that both methods were used to generate comparative estimates of abundance in 2006, and while these two estimates were similar, we chose to include them both as observations of total abundance in 2006. Total abundance was estimated each year with uncertainty, and we incorporated this uncertainty into the integrated population model as described below.

Calf Counts

Similar to the total abundance estimates of gray whales, calf production estimates are generated using shore-based counts of northbound migrating female whales with calves. Surveys take place from early March to late May at Piedras Blancas, in central California. Two early estimates of calf production were generated in 1980 and 1981 (*42*), and surveys were conducted continuously from 1994 – 2022 with the exception of 2020, when the survey was halted due to COVID-19 impacts (*25*).

Strandings

Documentation of stranded gray whales in the United States along the west coast of North America are reported opportunistically to the National Oceanic and Atmospheric Administration's National Marine Fisheries Service. For each gray whale stranding reported to the U.S. Marine Mammal Stranding Network, the authorized responding agency is required to complete a Marine Mammal Stranding Report – Level A data form (NOAA Form 89-864; OMB No. 0648-0178; form available at https://www.fisheries.noaa.gov/national/marine-life-distress/level-data-collection-marine-mammal-stranding-events). Level A data include details of each stranding (*e.g.*, species, date, stranding location, carcass condition, sex, length, examiner, signs of human interaction). While reports of stranded whales are recorded from Mexico and Canada, effort and reporting frequency of stranded whales is historically more consistent along the U.S. west coast and Alaska. During periods when an Unusual Mortality Event is declared, additional resources are available to increase survey effort for strandings in Mexico and Canada, but we chose to only include stranding records from the U.S. west coast and Alaska as a data source given the greater consistency in reporting. Within the U.S. Marine Mammal Strandings database, there was a major change to reporting and record keeping of strandings starting in 1990. In addition, survey effort for cetacean strandings in Alaska increased in the early 2000s. We therefore considered counts from 1974 – 1989, 1990 – 2000, and 2001-2022 to be three separate sampling periods as described below. The final U.S. Marine Mammal Stranding data used in this paper were extracted from the database on 05 October 2022 and data through August 31, 2022 are included.

In addition to total strandings numbers, we determined the number of stranded individuals with evidence of human interactions in the form of vessel strike and fishing gear entanglement injuries as recorded in the Level A data. The Findings of Human Interaction data field in the Level A data does not represent cause of stranding or cause of death (https://media.fisheries.noaa.gov/dam-migration/examiners_guide_2023.pdf). The cause of death is only determined for a very small subset of stranded individuals that receive internal examinations or complete necropsies, so confidently assigning an anthropogenic-origin mortality to a stranded whale based upon the presence of anthropogenic injuries listed on the Level A form is not possible. However, we reason that if many more whales are dying as a result of interactions with fishing gear (e.g. due to distributional changes caused by a marine heatwave; Samhouri et al. 2021) or vessel strikes, then proportionally more strandings would have evidence of human interactions. We incorporated counts of stranded gray whales with and without evidence of human interactions in the Level A data into the model as proxies for natural and anthropogenic mortality as described below.

Body Condition

We included two aerial photogrammetry datasets on gray whale body condition in our analyses. The first was collected from fixed wing aircraft along the coast of central California from the Channel Islands in the south to Monterey in the north, as described in Perryman & Lynn (2002). These aerial body condition surveys were conducted both in January, coinciding with the southbound migration, and in March, coinciding with the northbound migration. The survey period spanned 1987 – 2013, although aerial surveys were not conducted every year. The second

body condition dataset was collected using uncrewed aerial systems (drones) at Piedras Blancas during the northbound migration period only, and focused primarily on mother/calf pairs. Drone body condition surveys were conducted from 2015 – 2019, using methods described in (*44*). For our metric of body condition, we used the ratio of the maximum width of a whale to its length. Many recent studies of cetacean body condition have used the ratio of a whale's width at a fixed relative distance along the body to its length as a metric of condition (*18*, *45*, *46*), or more comprehensive indices such as body volume or body area (*47–49*). While these approaches are likely more consistent and therefore preferable to our metric of maximum width divided by length, only length and maximum width measurements were available from the archival fixed-wing photogrammetry datasets of gray whales from 1988-2013 (*26*). For measurements from the drone body condition dataset in 2015-2019, we compared the maximum width to body length ratio with the ratio of width at 50% of the body length to body length, which had a correlation coefficient of 0.77. The body condition metrics calculated using maximum width may be less accurate reflections of nutritive condition than those using width at a fixed relative distance along the body, however given the strong correlation between the two metrics we used the ratio of maximum width to length, allowing us to include body condition metrics from 1988 – 2019 in our analyses. We excluded visibly pregnant females from the dataset as the maximum width of these individuals is likely more closely related to pregnancy-related changes to body shape rather than nutritive condition. In addition, we excluded calves migrating north with their mothers from the body condition dataset, as their condition metrics were likely to be correlated with the condition metrics of their mothers (*48*, *50*), which could confound analyses including those paired samples.

Covariates

We considered three covariates that could potentially explain gray whale population dynamics. Whereas previous studies have evaluated a wide range of environmental variables that could be correlated with gray whale population dynamics (e.g. birth rates; Perryman et al. 2020), we focused on factors that could plausibly have direct causal influences on survival, condition and birth rates. Specifically, we considered metrics of access to Arctic feeding grounds and prey availability at these feeding grounds. While gray whales feed throughout the northern Bering Sea, Chirikov Basin, and Chukchi Sea, our bounding box (Figure S1) covers the region that has historically been a consistent hotspot for observations of foraging gray whales (*12*, *51*). As the Arctic has warmed and remained ice-free for longer, gray whales have expanded their feeding distribution as far north as point Barrow (*12*, *23*). However, the distribution of high-density amphipod prey in these more northerly feeding grounds is far more constrained than in the primary historical gray whale feeding areas between St. Lawrence Island and Point Hope (*12*). Despite a northward expansion, these primary feeding areas in the northern Bering and southern Chukchi sea have remained consistent hotspots for observations of feeding gray whales, with fluctuations in sighting rates that appear to align with benthic prey availability and sea ice cover (*12*, *23*, *51*). We therefore focus on this area for our covariate selection as we posit that it best represents prey availability on key foraging grounds for gray whales, while also providing a consistent long-term time series of in-situ benthic prey collection that spans almost the entire gray whale abundance time series. Within this focal area, we calculated the number of days in each year between the date when sea ice first drops below and first advances past 50% concentration. "Days of open water" was calculated using daily or alternating day sea ice

concentration layers from Sea Ice Index dataset (SII, version 3, ftp://sidads.colorado.edu/DATASETS/NOAA/G02135/north/daily/geotiff/, accessed May 26, 2021) produced by the NOAA National Snow and Ice Data Center (NSIDC) at a nominal resolution of 25 km at 70ºN in polar stereographic projection (EPSG: 3411). Aerial survey counts from the northeast Chukchi Sea indicate that above 50% sea ice concentration gray whale occurrence drops off precipitously, while below this 50% threshold it appears that gray whales can begin to access their summer feeding grounds (*23*). Within the same bounding box we generated an annual index of mean benthic crustacean biomass using in-situ benthic sediment samples collected by the PACMARS and DBO programs between 1970 and 2019 (*28*). Gray whales have been documented feeding on diverse prey assemblages in the Arctic, however their primary prey targets are benthic amphipods and other infaunal crustaceans (*12*). In many of the historically important Arctic gray whale feeding grounds, benthic crustacean abundance has remained stable or increased. However, the species composition has shifted away from the tube building benthic amphipods that are highest in lipid content and therefore highest value prey for gray whales (*12*). As such, we chose to use benthic crustacean biomass (grams of Carbon per cubic meter) as a more direct indicator of benthic prey availability and quality rather than abundance, which may not capture changes in prey quality. Moore et al. (2022) suggest that during periods of potentially low benthic prey availability, gray whales may shift foraging tactics to pelagic habitats, targeting krill and other zooplankton. We therefore included a metric of pelagic zooplankton density from the ECCO Darwin global ocean model (*29*). We used the total density of zooplankton at 5m water depth from the July model time step, within the same bounding box as ice access and benthic crustacean biomass (Figure S1). All covariates were lagged by one year in the model to refer to the prior foraging season. For example, carrying capacity in 2020 was related within the model to the covariate values from summer 2019, which would presumably influence survival, reproduction, and nutritive condition during the following winter and spring. A wider range of lag periods has previously been considered in studies relating gray whale reproductive output to environmental conditions including sea ice extent, and there is biological and empirical support for environmental conditions and feeding opportunities being most relevant during the gestation period (which occurs during the previous summer feeding period), rather than during pre-breeding periods (which would occur at a 2-year lag instead) (*22*).

Integrated Population Model

Process Model

The population dynamics process in our model is described by a discrete logistic growth equation, with a modification such that carrying capacity is variable and indexed by time:

$$N_{t+1} = N_t + rN_t\left(1 - \frac{N_t}{K_t}\right)$$

where N is the model-estimated total abundance of eastern North Pacific gray whales in year t, r is the population's intrinsic maximum growth rate, and K is the carrying capacity in year t. We modified this form of the equation to more easily incorporate births, deaths, and body condition observations:

$$N_{t+1} = N_t * (1 + B_t - M_t)$$

Where *B* is the annual birth rate and *M* is the annual mortality rate in year *t*. Logit-transformed birth rate and nutritive condition were modeled with linear relationships to abundance relative to annual carrying capacity, thus accounting for density dependent effects on vital rates:

$$logit(B_t) = \hat{B} - \beta_B * \frac{N_t}{K_t}$$

And

$$logit(C_t) = \hat{C} - \beta_C * \frac{N_t}{K_t}$$

Where C is the southbound nutritive condition of the population in year *t*, $\hat{B}$ and $\hat{C}$ determine the base birth rate and nutritive condition when abundance is far below carrying capacity, and β is a vector of parameters determining the effects of density dependence on vital rates. Our model tracks mortality from natural and anthropogenic sources separately using a proportional hazards formulation:

$$h_{N,t} = e^{\hat{\gamma}_E + \beta_E * \frac{N_t}{K_t}}$$

And

$$h_{A,t} = e^{\hat{\gamma}_A + \eta_t}$$

And

$$M_t = 1 - e^{-(h_{E,t} + h_{A,t})}$$

Where *h* is the instantaneous hazard rate for either natural mortality *E* or anthropogenic mortality *A* in year *t*, $\hat{\gamma}$ is the base log hazard rate for natural or anthropogenic mortality, β_E is the log hazard ratio associated with a unit increase in population density (relative to annual *K*) and thus determines the strength of density dependent variation in natural mortality, and η is a random effect determining year-to-year variation in anthropogenic hazards. Maximum growth rate *r* from the original logistic equation can then be calculated from the maximum birth rate and minimum mortality rate at low population densities (~ 1% of *K*):

$$logit(B_{max}) = \hat{B} - \beta_B * 0.01$$

and

$$M_{min} = 1 - e^{-e^{\hat{\gamma}_E + \beta_E * 0.01}}$$

And

$$r = B_{max} - M_{min}$$

We set an informative prior distribution for *r* of N[0.1, 0.001], informed by previous estimates of gray whale r_{max} values (*21*).

Annual carrying capacity was estimated as a function of environmental covariates such that:

$$K_t = \widehat{K} * e^{\sum Cov_{c,t} * \beta_c + \epsilon_t}$$

Where K is instantaneous carrying capacity in year t, $\widehat{K}$ is a constant representing the median expected annual K value, Cov_c is Z-scored covariate c (centered and scaled to have mean of 0 and unit variance), β_c is a fitted parameter that determines the effect of covariate c on carrying capacity, and ϵ represents the effect of environmental stochasticity, or unexplained variation in annual K_t, treated as a random normal variable with mean of 0 and standard error of σ_k. We note that missing values of covariates were estimated using auto-regressive techniques, as explained below. We set $\widehat{K}$ = 24,500 based on iteratively re-fitting the model to find the value of $\widehat{K}$ that ensured that expected K_t (calculated from the above equation) was identical to the numerically derived equilibrium abundance calculated by recursively solving the process model with the current values of Cov_c and ϵ until N stabilized (following methods described below in section "Estimating Long term K").

The process model could have been formulated in a variety of ways to explain variability in vital rates and abundance of gray whales. For example, rather than applying covariate effects to explain annual carrying capacity K_t, they could instead be applied to the intrinsic population growth rate parameter r, or to vital rates independently (birth rate, survival rate, nutritive condition) with separately estimated effects. Further, the effects of density dependence could be eliminated altogether by removing carrying capacity from the equation and allowing population fluctuations to be governed entirely by covariates and random effects. However, a preliminary examination of the survey data indicated a significant negative relationship between the log of estimated annual growth rates and abundance (linear model t = 2.492, df=53, p = 0.0159; Figure S9), providing empirical support for density-dependent population dynamics. Annual growth rates also became more variable at higher abundance, with sharp declines of ~10% or more only occurring when the gray whale population was at high abundance levels (Figure S9), suggesting that the magnitude of environmentally-driven booms and busts are density dependent. Most importantly, we believe that modeling covariate effects on K rather than r most closely approximates biological reality. The Bering and Chukchi seas are the primary feeding ground for the vast majority of gray whales (>95%). As such, the conditions in these spatially restricted feeding areas directly impact food availability for almost the entire eastern North Pacific population. We therefore posit that the quality, quantity, and access to that prey will have a greater influence on vital rates when there is high intra-specific competition for limited resources (i.e. at high levels of gray whale abundance). Applying covariate effects to K therefore allows vital rates to be governed by a combination of environmental conditions and intrinsic density dependence, with environmental conditions having a weaker effect on vital rates when gray whale abundance is low.

Observation Model

Observations of annual abundance are included from Granite Canyon survey estimates:

$$n_t \sim Normal[N_t, \sigma_{n_t}]$$

where n is the median or maximum likelihood estimate of abundance in year t, normally distributed around the model-estimated true total abundance with uncertainty σ associated with

each estimate *n* in year *t*, which is either the standard deviation of the posterior distribution for estimates generated using Bayesian methods (*40*) or the standard error of the estimate for those generated using maximum likelihood methods (*39*). Note that Granite Canyon abundance estimates are indexed to year *t* such that the survey period begins in December of year *t-1* and ends in February of year *t* (e.g. the December 2019 – February 2020 survey is considered the abundance estimate for year 2020).

Model estimated annual births *b* are calculated as birth rate *B* multiplied by the annual estimated abundance *N*:

$$b_t = B_t * N_t$$

Empirical estimates of calf production are incorporated into the model as observations of the true number of births:

$$Calves_t \sim Normal[b_t, \sigma_{Calves_t}]$$

where *Calves* refers to the median estimated calf production from Piedras Blancas surveys in year *t*, and σ is the standard deviation of the posterior distribution of each estimate.

The annual number of deaths attributed to natural or anthropogenic mortality is estimated using strandings as a proxy for mortality, such that:

$$Exp.Str_{E,t} = N_t * M_t * \frac{h_{E.t}}{h_{E,t} + h_{A,t}} * P.Str_p$$

and

$$Exp.Str_{A,t} = N_t * M_t * \frac{h_{A.t}}{h_{E,t} + h_{A,t}} * P.Str_p$$

Where *Exp.Str* is the number of dead whales expected to be observed as strandings in year *t* with evidence of human interactions (*A*) or no evidence of human interactions (*E*), which is the product of total mortality *M*, abundance *N*, the proportional contribution to total hazards (*h*) from anthropogenic or natural mortality, and the probability of a dead whale being detected as a stranding in California, Oregon, Washington or Alaska (*P.Str*) during time period *p* associated with year *t*. We included three separate stranding detection periods: 1970-1990, 1990-2000, and 2000-2022 based on expert consultation with NOAA national and regional strandings coordinators as described above. We assume that the probability of a dead whale being detected as a stranding is equal for whales that die of natural causes and those that die of anthropogenic causes, as gray whales have a very near-shore distribution in comparison to other baleen whales. Thus, we do not expect whales that die of anthropogenic causes to be distributed in closer proximity to anthropogenic threats (e.g. coastal vessel traffic and fishing effort) where they may be more likely to wash ashore than those that die of natural causes, which might reasonably create a bias in favor of anthropogenic mortality detection in other species of baleen whale that have more offshore distributions. We used vague prior distributions Beta[1,1] for stranding

proportions *P.Str*. The empirically observed number of strandings *str* with either evidence of human interactions or no evidence of human interactions were assumed to be distributed following a Poisson distribution around the expected number of strandings of each type:

$$str_{E,t} \sim Poisson[Exp.Str_{E,t}]$$

And

$$str_{A,t} \sim Poisson[Exp.Str_{A,t}]$$

In short, there are three model-estimated probabilities of dead whales stranding and being recorded—one for the low-effort survey period pre-1990 and two for the higher effort periods post-1990—that are used to transform observed strandings into overall mortality and thus inform the contributions of density-dependent versus anthropogenic mortality.

We incorporate observations of body condition into the model by assuming that body condition measurements are beta distributed around the mean expected condition during the southbound migration:

$$Cond_{SB,i} \sim Beta[C_t * \tau_{SB}, (1 - C_t) * \tau_{SB}]$$

where *Cond* is the measured body condition of whale *i* in year *t*, *C* is the model-estimated average of southbound condition, and τ_{SB} is the precision parameter of the beta distribution, estimated as part of model fitting. To incorporate northbound body condition measurements, we applied a proportional correction factor to southbound condition *C*, as northbound migrating whales should be in worse condition after fasting for an additional several months:

$$C_{NB,t} = C_t * NB.Adjust$$

And:

$$Cond_{NB,i} \sim Beta[C_{NB,t} * \tau_{NB}, (1 - C_{NB,t}) * \tau_{NB}]$$

Where *NB.Adjust* is a model-estimated correction factor bounded by [0,1], C_{NB} is the population mean northbound condition, and τ_{NB} is the fitted precision parameter of the beta distribution. Note that there are no known repeated measurements for individually identifiable whales, and thus index *i* simply indicates a unique body condition measurement.

Our study period spans 1968 – 2022, but our three candidate Arctic environmental covariates do not span the full study period, and have periodic data gaps. To account for missing data, we fit an auto-regressive random walk process model to the covariate data within the integrated population model to estimate covariate values for data gaps. We assumed that recorded covariate values were perfectly observed, while unobserved covariate values were estimated as:

$$Cov_{C,t} \sim Normal[Cov_{c,t-1}, \sigma_c]$$

where *Cov* is the observed or, for years with no data, model-estimated covariate value at time *t*, for covariate *C*, and σ_C is a fitted parameter specifying process error for covariate *C*. Recorded covariate values were scaled to mean 0 and standard deviation 1 (Z-scored) prior to inclusion in the model, and then during model fitting (after auto-regressive estimation of missing data) were Z-scored a second time. This placed all covariates, including both observed and model-estimated values, on the same scale, thereby making model-estimated coefficients for covariate effects directly comparable. We note that, due to the second Z-scoring step, even observed covariate values had a small amount of variance reflecting variability in the model-estimated values for missing data years.

Estimating Long term K

The annual K_t values can be interpreted as the equilibrium abundance that would eventually be achieved were environmental conditions and stochastic effects to remain indefinitely fixed at the values observed for the current year. However, because environmental conditions are dynamic, we recognize that no single value of annual K_t is representative of average equilibrium abundance over the longer-term. We instead used iterative simulations to calculate long-term *K* as a derived parameter, which we define as the average equilibrium abundance (averaged over a sufficiently long period of time) that would be expected if future variation in environmental conditions and stochastic effects correspond to the observed distributions over the study period. This definition of long-term *K* thus incorporates and accounts for environmental stochasticity.

For each simulation, we randomly sampled a value for each process model parameter from the joint posterior. We then projected the process model forward for 200 years: for each year, we drew random values of each covariate from the empirically derived sampling distributions (which we fit to observed values over the study period), and we drew random values for ϵ from the normal distribution defined by hyperparameter σ_K. The first 100 years of each simulation were used to allow N_t to reach a dynamic equilibrium, and thus discarded, and we saved the average value of N_t over the second 100 years of the simulation. These simulations were repeated 10,000 times, and we used the resulting distribution of average equilibrium abundance values as the posterior distribution of long-term *K*.

Model Fitting

We used vague prior distributions for all model parameters, which we define as weakly informed based on biological feasibility but having no information specific to this analysis. We used Normal[0, 2.5] priors for log-hazard base rate parameters $\hat{\gamma}$ and for logit base parameters $\hat{B}$ and $\hat{C}$. We used Cauchy[0, 2.5] priors for unconstrained β parameters and used half-Cauchy[0, 2.5] priors for β parameters logically constrained to be positive, as well as for variance and precision parameters. We note the Cauchy distribution has been suggested as an effective, uninformative prior because it has a taller peak than the Normal distribution, is leptokurtic ("fat tailed"), and has no defined mean, and thus provides wide potential bounds on parameter space, a tendency to shrink towards 0 for non-significant parameters, and minimized influence of the prior on the estimation of the posterior (*52*). For those parameters constrained to the 0-1 range, we used flat Beta priors with parameters a = b = 1. In the case of initial population size ($N_{t=0}$) we used a weakly informative gamma distribution with shape parameter = 6.75 and rate parameter =

0.0005, as this distribution encompassed a broad range of values consistent with all previously reported historical estimates.

The observed data variables constrained the possible values of unknown parameters in the process model, allowing us to estimate posterior distributions for these parameters using standard Markov Chain Monte Carlo (MCMC) methods. We used R (*53*) and Stan software (*54*) to code and fit the model, saving 20,000 samples after a burn-in of 1000 samples. We evaluated model convergence by graphical examination of trace plots from 20 independent chains and by ensuring that the Gelman-Rubin convergence diagnostic (R-hat) was <1.01 (*55*) and the effective sample size was >500 for all fitted model parameters. We conducted graphical posterior predictive checking to evaluate model goodness of fit, ensuring that out-of-sample predictive distributions of abundance, body condition, calf counts, and stranded carcasses were fully consistent with the equivalent empirical distributions of observed data.

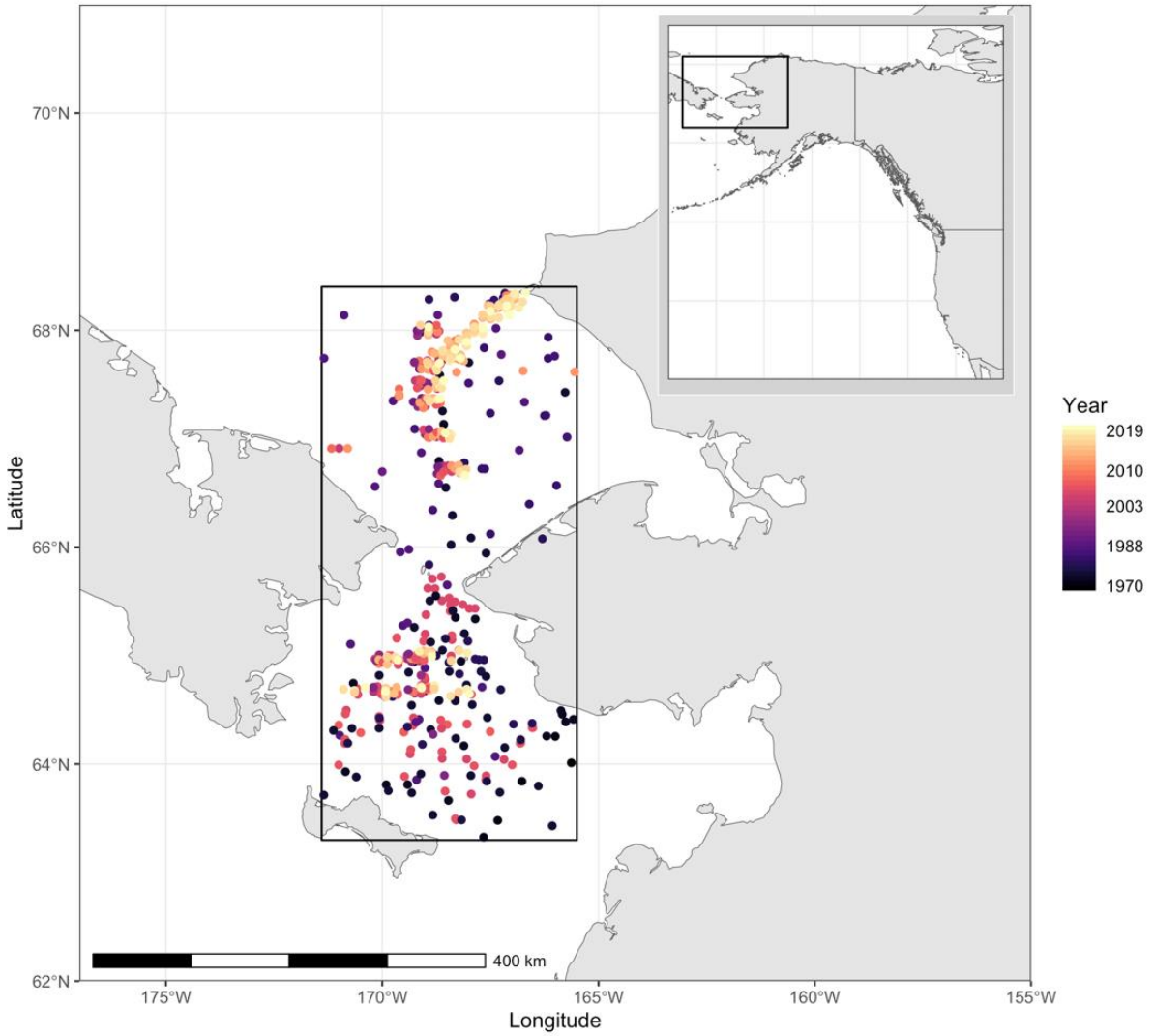

Figure S1: Map of Arctic environmental covariate survey areas and primary gray whale feeding areas in the Bering and Chukchi seas. The black box in the main panel indicates the bounding box for all covariates, including benthic crustacean biomass (plotted), number of days of ice access, and average zooplankton density. Benthic infaunal sampling locations are shown from sampling sites within the bounding box, with color representing sampling year. Plotted sampling locations are jittered for visibility, as many locations had repeated sampling across years. Black box in the inset map indicates the primary map area.

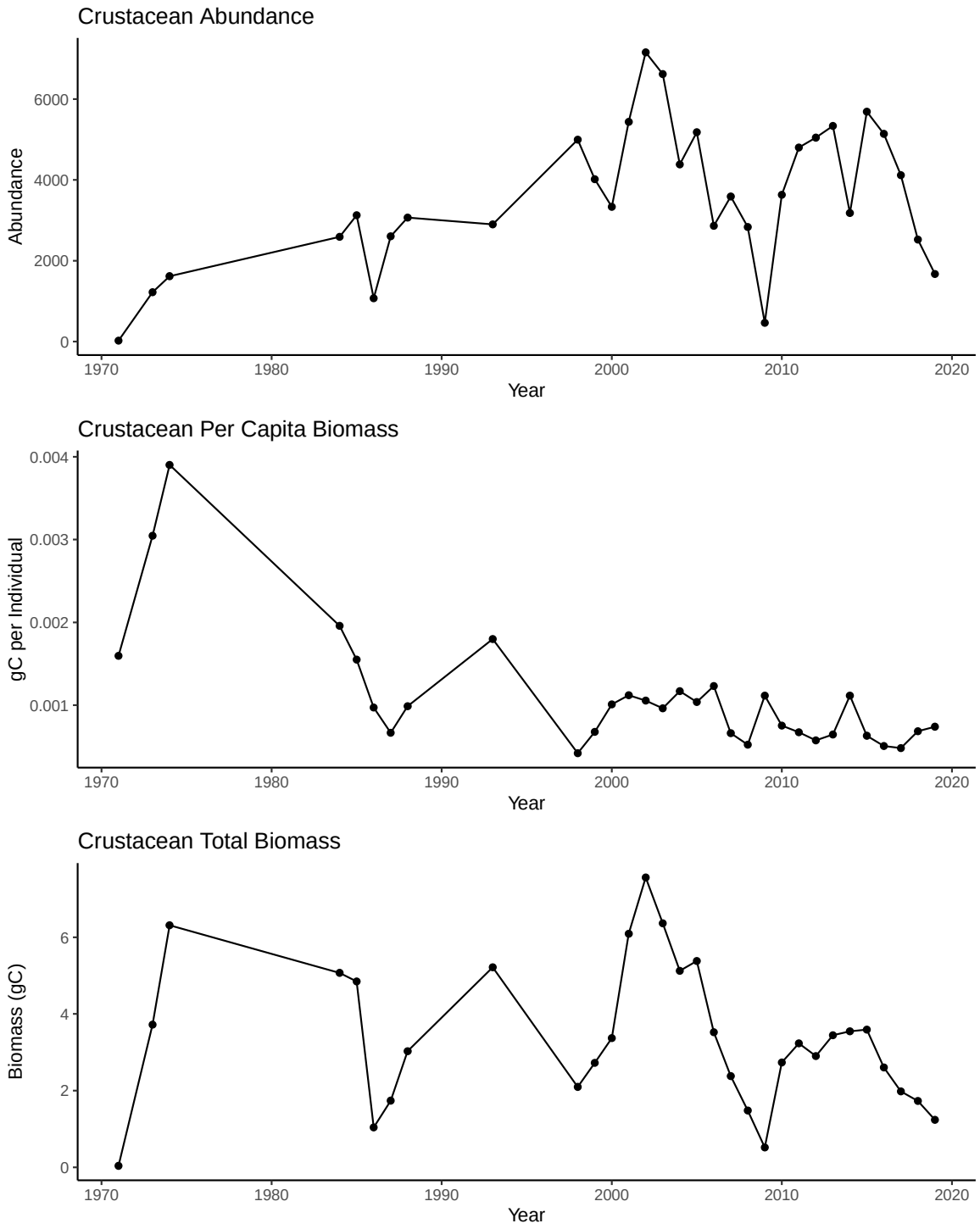

Figure S2: Infaunal benthic crustacean time series from gray whale feeding hotspots in the Bering and Chukchi seas. Top: mean crustacean abundance per sample within the study area. Middle: mean crustacean abundance per sample divided by mean crustacean biomass per sample. Bottom: mean crustacean biomass in grams of carbon per sample.

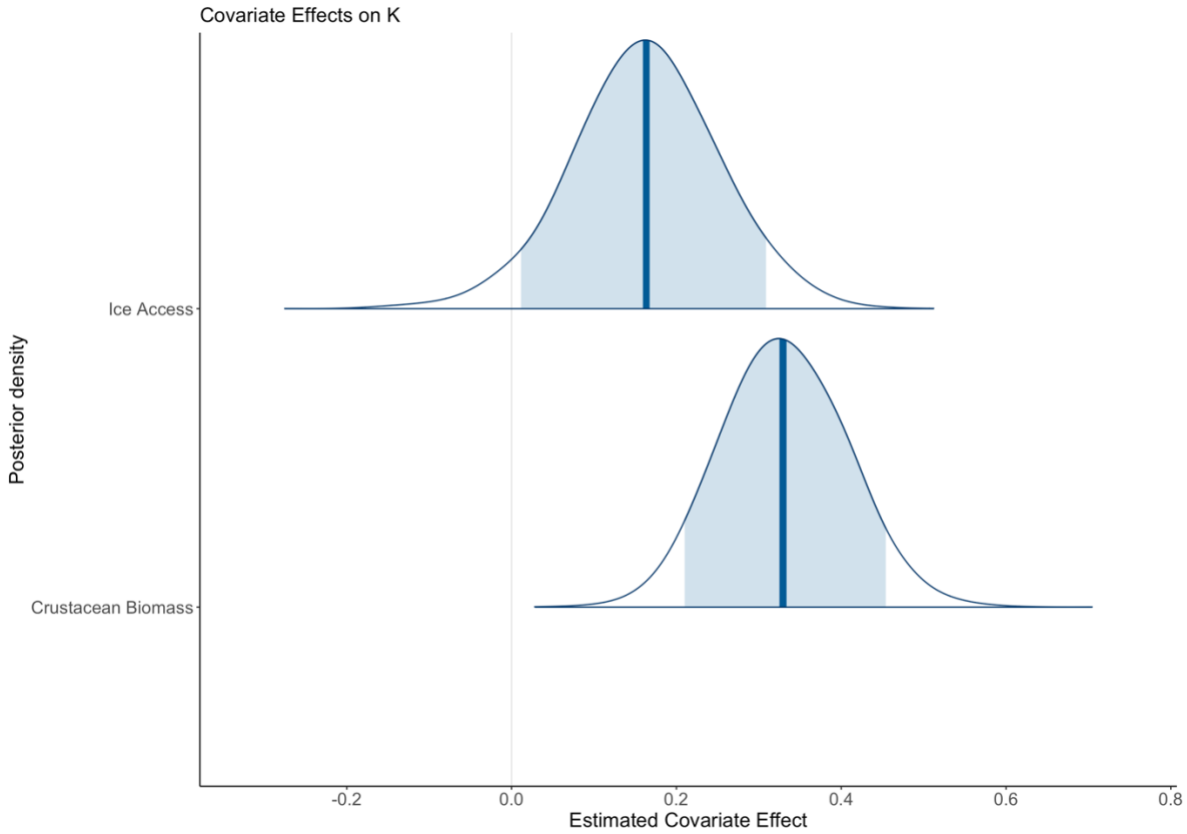

Figure S3: Posterior distributions of covariate effects on annual carrying capacity, for the model formulation with crustacean biomass and ice access. Vertical blue bars indicate the median, and light blue polygons the 90% highest posterior density intervals of the posterior distributions.

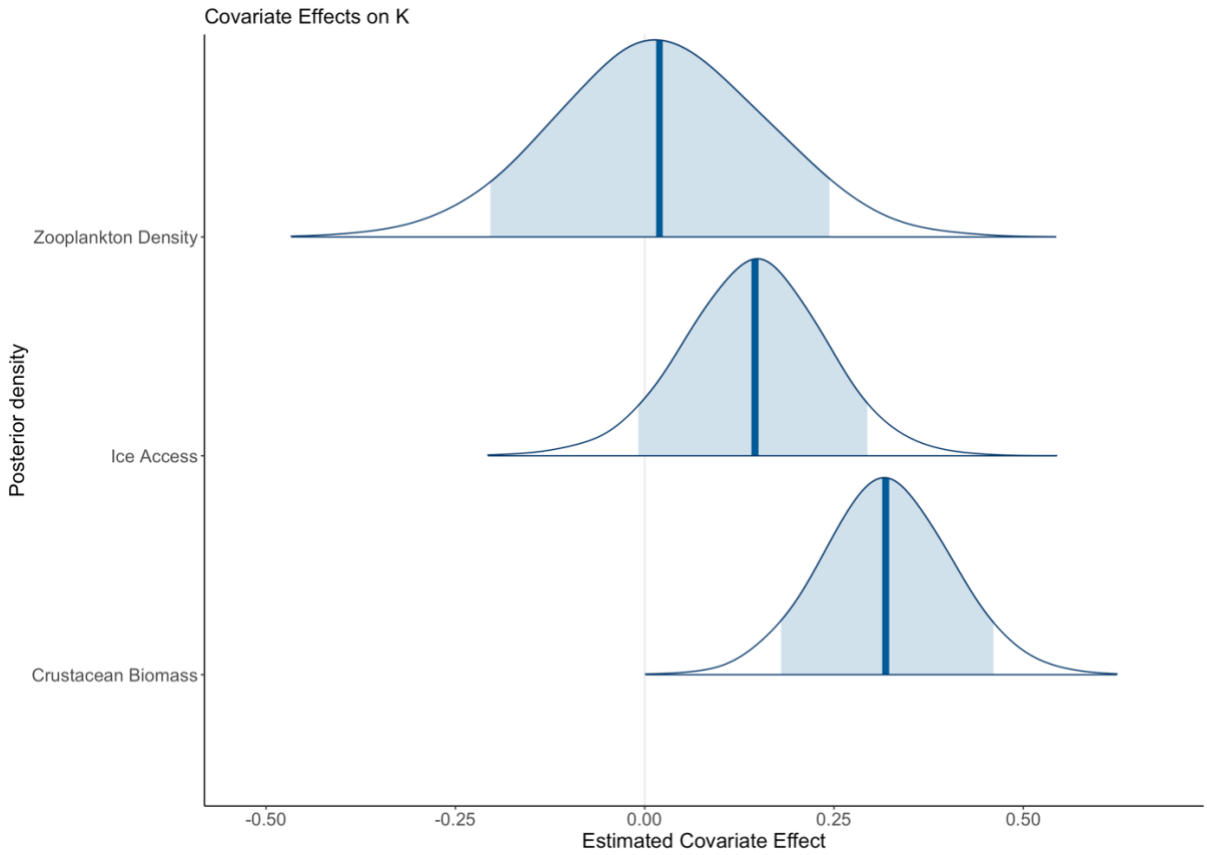

Figure S4: Posterior distributions of covariate effects on annual carrying capacity, for the model formulation with crustacean biomass, ice access, and zooplankton density. Vertical blue bars indicate the median, and light blue polygons the 90% highest posterior density intervals of the posterior distributions.

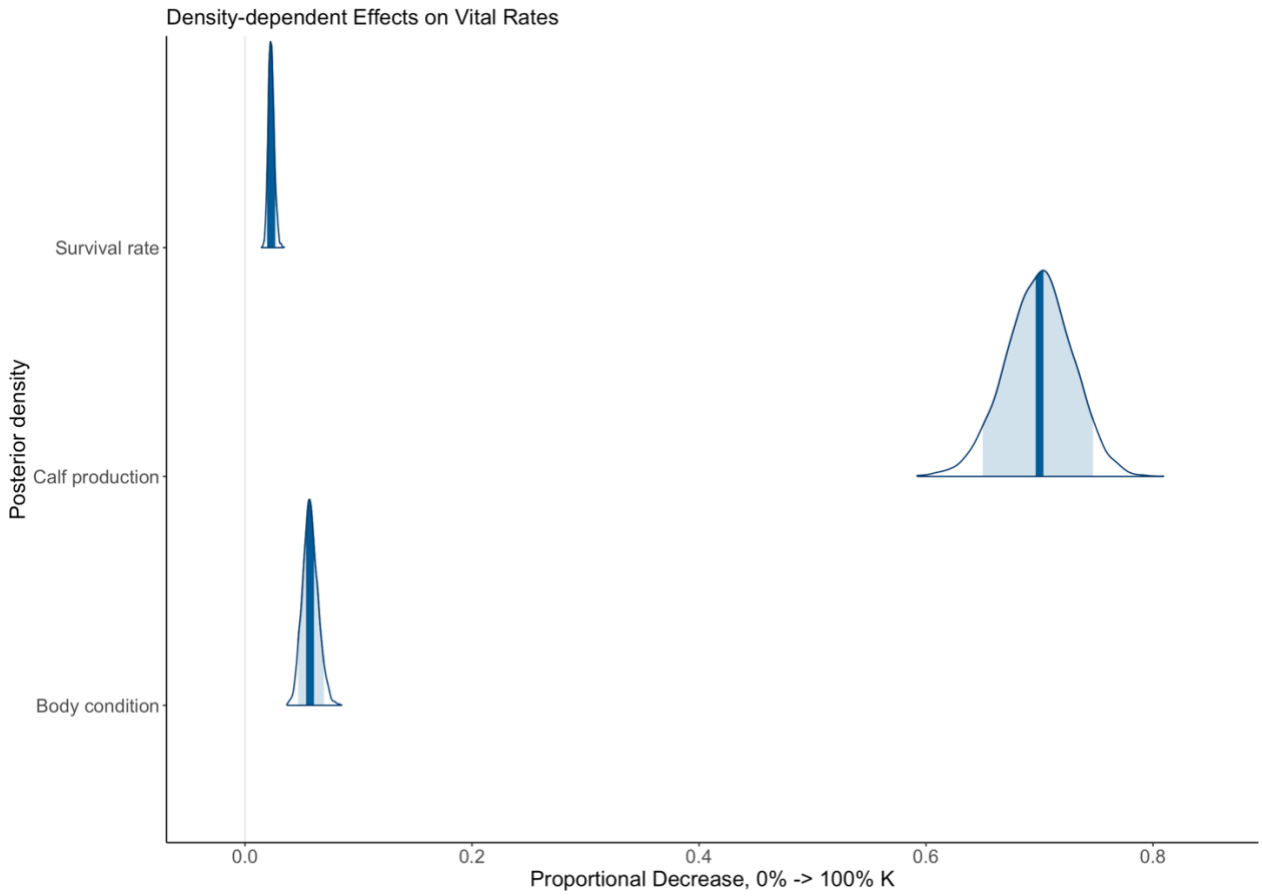

Figure S5: Standardized density-dependent effects on vital rates. Proportional decrease in vital rates over a change in annual abundance (N) relative to annual carrying capacity (K) from N/K = 0 to N/K = 1. Vertical blue bars indicate the median, and light blue polygons the 90% highest posterior density intervals of the posterior distributions.

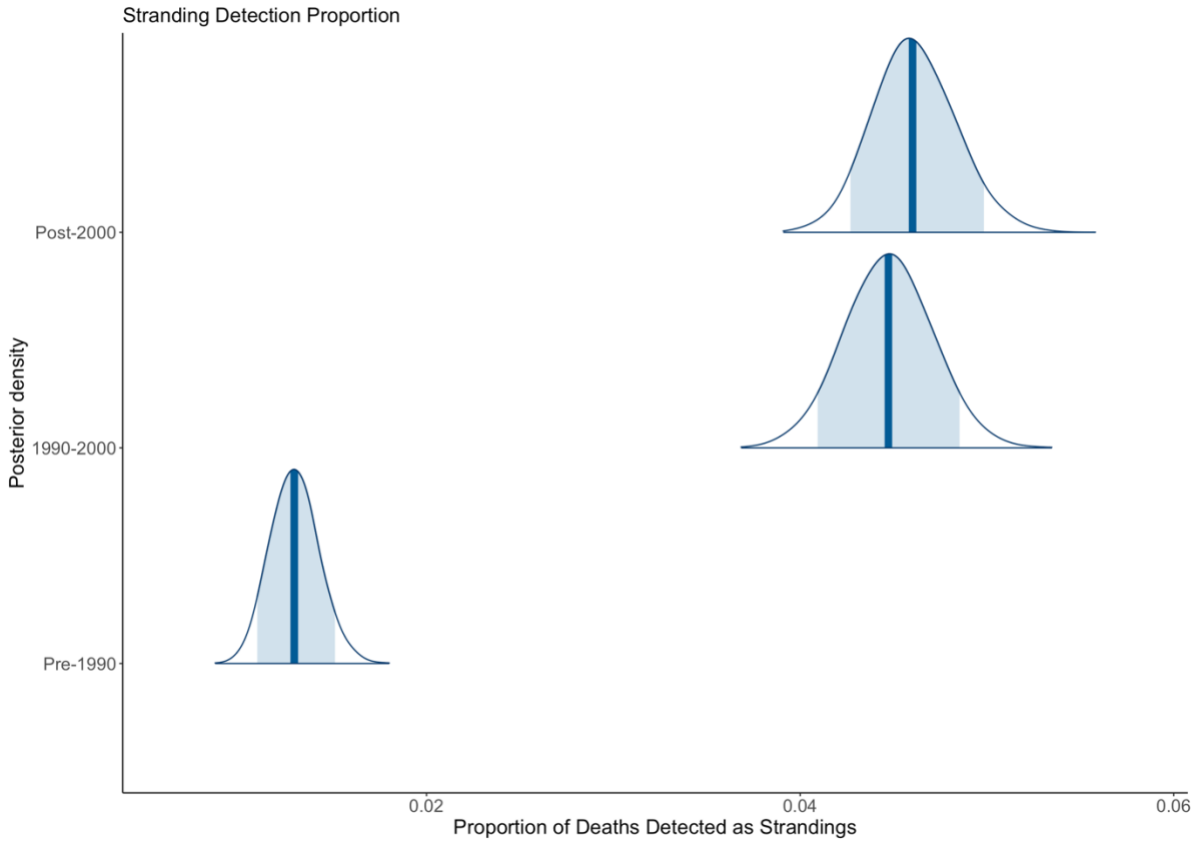

Figure S6: Model-estimated proportion of deaths recovered as strandings for the three stranding detection periods 1970-1990, 1990-2000, and 2000-2022. Vertical blue bars indicate the median, and light blue polygons the 90% highest posterior density intervals of the posterior distributions.

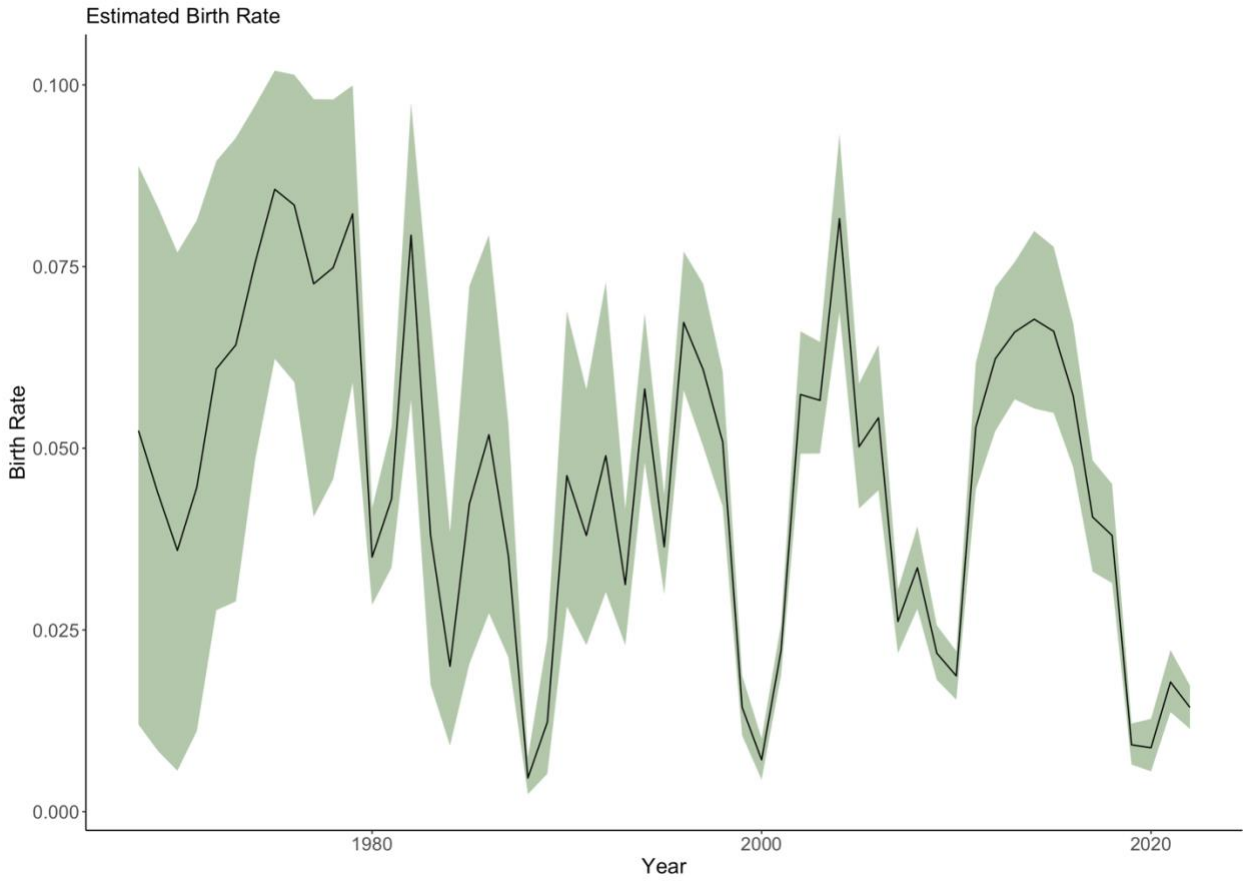

Figure S7: Model-estimated birth rates. The black line indicates the annual median model-estimated birth rate, and the green ribbon indicates the 95% credible intervals of the posterior estimate. Estimates of annual calf production (not shown), which were included as observations of births in the population dynamics model, were available in 1980-81, 1994-2019, and 2021-22.

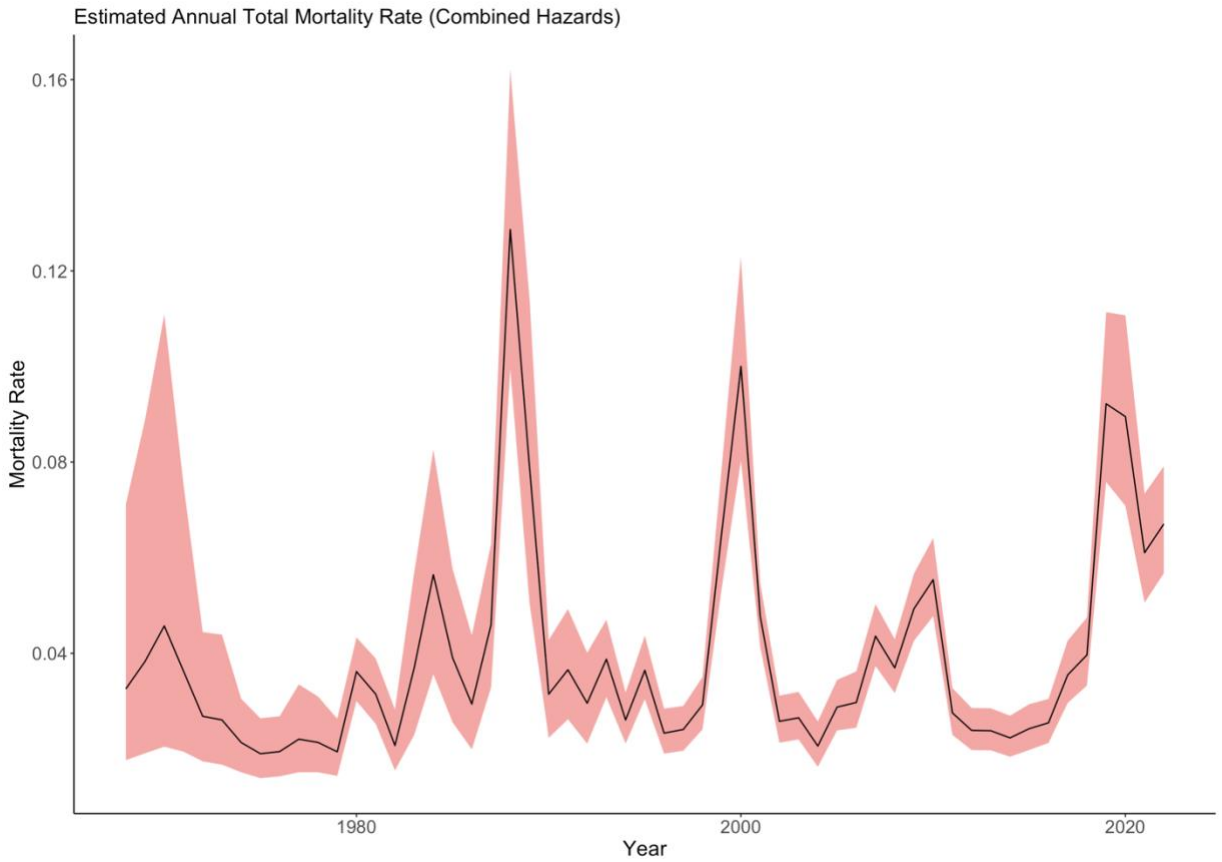

Figure S8: Model-estimated mortality rates. The black line indicates the annual median model-estimated mortality rate (combined anthropogenic and natural hazards), and the green ribbon indicates the 95% credible intervals of the posterior estimate.

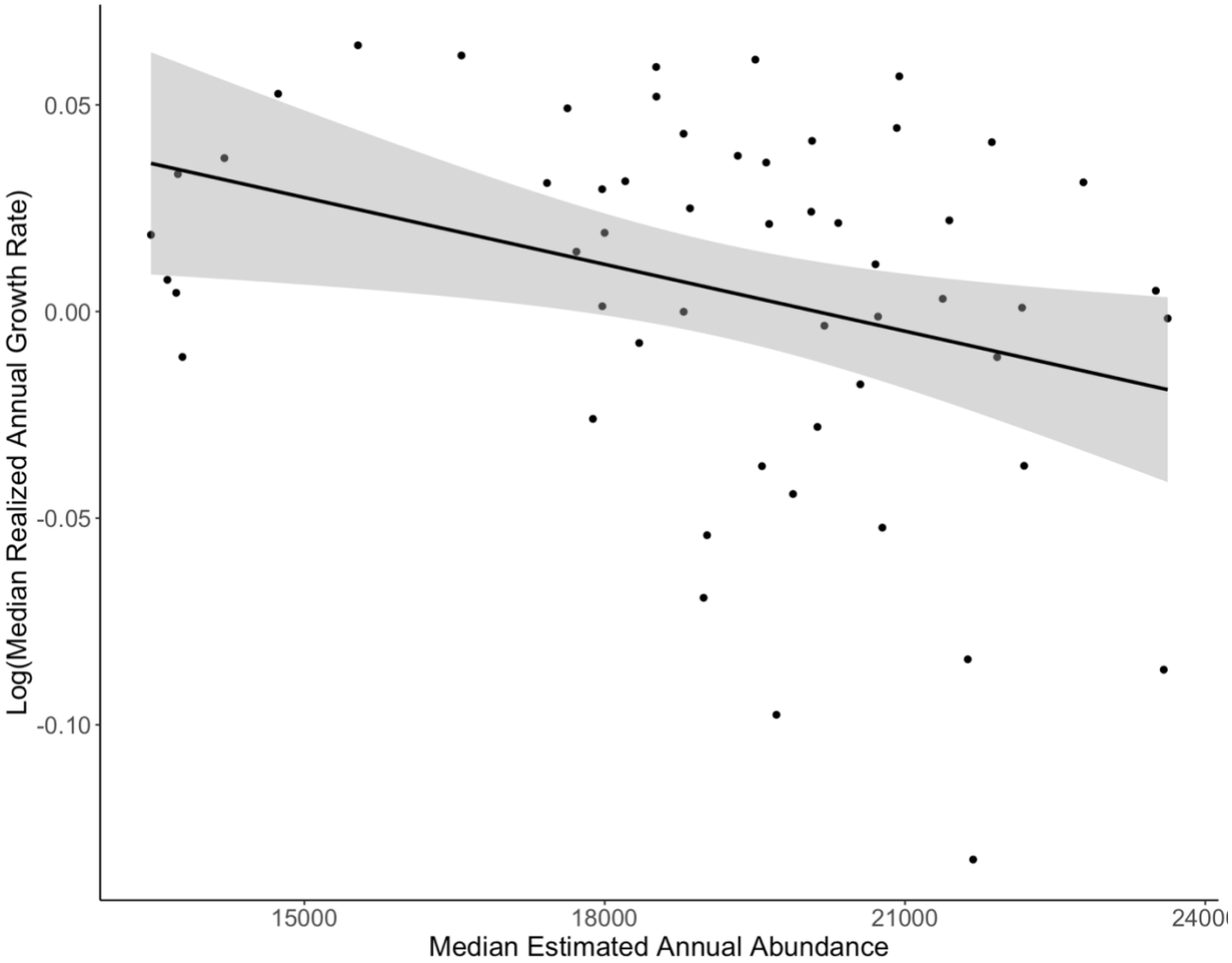

Figure S9. Density-dependent effects on population growth rates. The y-axis represents the log of the median realized annual growth rates (i.e. N_{t+1} / N_t, often represented by λ). Values below zero indicate population decline whereas those above 0 indicate growth. The x-axis represents the annual abundance of the population (N_t). The black line is a simple linear regression with confidence intervals plotted as the gray polygon. The more extreme negative growth rates at greater abundance levels indicate interactive effects of environmental conditions and intra-specific competition.

References and Notes

1. R. C. Highsmith, K. O. Coyle, High productivity of northern Bering Sea benthic amphipods. *Nature* **344**, 862–864 (1990).

2. A. M. Springer, C. P. McRoy, M. Flint, The Bering Sea Green Belt: Shelf-edge processes and ecosystem production. *Fish. Oceanogr.* **5**, 205–223 (1996).

3. J. M. Grebmeier, L. W. Cooper, H. M. Feder, B. I. Sirenko, Ecosystem dynamics of the Pacific-influenced Northern Bering and Chukchi Seas in the Amerasian Arctic. *Prog. Oceanogr.* **71**, 331–361 (2006).

4. K. J. Kuletz, M. C. Ferguson, B. Hurley, A. E. Gall, E. A. Labunski, T. C. Morgan, Seasonal spatial patterns in seabird and marine mammal distribution in the eastern Chukchi and western Beaufort seas: Identifying biologically important pelagic areas. *Prog. Oceanogr.* **136**, 175–200 (2015).

5. J. M. Grebmeier, J. E. Overland, S. E. Moore, E. V. Farley, E. C. Carmack, L. W. Cooper, K. E. Frey, J. H. Helle, F. A. McLaughlin, S. L. McNutt, A major ecosystem shift in the northern Bering Sea. *Science* **311**, 1461–1464 (2006).

6. H. P. Huntington, S. L. Danielson, F. K. Wiese, M. Baker, P. Boveng, J. J. Citta, A. De Robertis, D. M. S. Dickson, E. Farley, J. C. George, K. Iken, D. G. Kimmel, K. Kuletz, C. Ladd, R. Levine, L. Quakenbush, P. Stabeno, K. M. Stafford, D. Stockwell, C. Wilson, Evidence suggests potential transformation of the Pacific Arctic ecosystem is underway. *Nat. Clim. Chang.* **10**, 342–348 (2020).

7. K. R. Arrigo, G. L. van Dijken, Continued increases in Arctic Ocean primary production. *Prog. Oceanogr.* **136**, 60–70 (2015).

8. K. M. Lewis, G. L. van Dijken, K. R. Arrigo, Changes in phytoplankton concentration now drive increased Arctic Ocean primary production. *Science* **369**, 198–202 (2020).

9. J. M. Grebmeier, K. E. Frey, L. W. Cooper, M. Kędra, Trends in benthic macrofaunal populations, seasonal sea ice persistence, and bottom water temperatures in the Bering Strait region. *Oceanography* **31**, 136–151 (2018).

10. J. M. Grebmeier, S. E. Moore, J. E. Overland, K. E. Frey, R. Gradinger, Biological response to recent Pacific Arctic sea ice retreats. *Eos* **91**, 161–162 (2010).

11. G. C. Pike, Migration and feeding of the gray whale (*Eschrichtius gibbosus*). *J. Fish. Res. Board Can.* **19**, 815–838 (1962).

12. S. E. Moore, J. T. Clarke, S. R. Okkonen, J. M. Grebmeier, C. L. Berchok, K. M. Stafford, Changes in gray whale phenology and distribution related to prey variability and ocean biophysics in the northern Bering and eastern Chukchi seas. *PLOS ONE* **17**, e0265934 (2022).

13. A. E. Punt, C. Allison, G. Fay, An examination of assessment models for the eastern North Pacific gray whale based on inertial dynamics. *J. Cetacean Res. Manag.* **6**, 121–132 (2004).

14. S. E. Alter, E. Rynes, S. R. Palumbi, DNA evidence for historic population size and past ecosystem impacts of gray whales. *Proc. Natl. Acad. Sci. U.S.A.* **104**, 15162–15167 (2007).

15. N. D. Pyenson, D. R. Lindberg, What happened to gray whales during the Pleistocene? The ecological impact of sea-level change on benthic feeding areas in the North Pacific Ocean. *PLOS ONE* **6**, e21295 (2011).

16. P. J. Clapham, S. B. Young, R. L. Brownell, Baleen whales: Conservation issues and the status of the most endangered populations. *Mammal Rev.* **29**, 37–62 (1999).

17. B. J. Le Boeuf, H. Pérez-Cortés M., J. Urbán R., B. R. Mate, F. Ollervides U., High gray whale mortality and low recruitment in 1999: Potential causes and implications. (*Eschrichtius robustus*). *J. Cetacean Res. Manag.* **2**, 85–99 (2000).

18. F. Christiansen, F. Rodríguez-González, S. Martínez-Aguilar, J. Urbán, S. Swartz, H. Warick, F. Vivier, L. Bejder, Poor body condition associated with an unusual mortality event in gray whales. *Mar. Ecol. Prog. Ser.* **658**, 237–252 (2020).

19. S. E. Moore, R. Jorge Urbán, W. L. Perryman, F. Gulland, M. Hector Perez-Cortes, P. R. Wade, L. Rojas-Bracho, T. Rowles, Are gray whales hitting "K" hard? *Mar. Mamm. Sci.* **17**, 954–958 (2001).

20. J. R. Brandon, A. E. Punt, "Assessment of the eastern stock of North Pacific gray whales: incorporating calf production, sea-ice and strandings data," paper SC/61/AWMP2 presented to the International Whaling Commission (IWC) Scientific Committee (2009).

21. A. E. Punt, P. R. Wade, "Population status of the eastern North Pacific stock of gray whales in 2009," US Department of Commerce, National Oceanic and Atmospheric Administration (NOAA) Technical Memo NMFS-AFSC-207, 43 (2009).

22. W. L. Perryman, T. Joyce, D. W. Weller, J. W. Durban, Environmental factors influencing eastern North Pacific gray whale calf production 1994–2016. *Mar. Mamm. Sci.* **37**, 448–462 (2020).

23. T. W. Joyce, M. C. Ferguson, C. L. Berchok, D. L. Wright, J. L. Crance, E. K. Braen, T. Eguchi, W. L. Perryman, D. W. Weller, The role of sea ice in the distribution, habitat use, and phenology of eastern North Pacific gray whales. *Mar. Ecol. Prog. Ser.* **709**, 141–158 (2023).

24. T. Eguchi, A. R. Lang, D. W. Weller, "Abundance and migratory phenology of Eastern North Pacific gray whales 2021/2022," US Department of Commerce, NOAA Technical Memorandum NMFS-SWFSC-668 (2022); .

25. T. Eguchi, A. R. Lang, D. W. Weller, "Eastern North Pacific gray whale calf production 1994-2022," US Department of Commerce, NOAA Technical Memorandum NMFS-SWFSC-667 (2022); .

26. W. L. Perryman, M. S. Lynn, Evaluation of nutritive condition and reproductive status of migrating gray whales (*Eschrichtius robustus*) based on analysis of photogrammetric data. *J. Cetacean Res. Manag.* **4**, 155–164 (2002).

27. G. Gailey, O. Sychenko, O. Tyurneva, Y. Yakovlev, V. Vertyankin, P. van der Wolf, K. Drozdov, I. Zhmaev, Effects of sea ice on growth rates of an endangered population of gray whales. *Sci. Rep.* **10**, 1553 (2020).

28. J. M. Grebmeier, L. W. Cooper, Benthic macroinfaunal and dominant taxa samples collected from Northern Bering Sea to Chukchi Sea, 1970–2019 (2023); https://arcticdata.io/catalog/view/doi%3A10.18739%2FA24T6F480.

29. D. Carroll, D. Menemenlis, J. F. Adkins, K. W. Bowman, H. Brix, S. Dutkiewicz, I. Fenty, M. M. Gierach, C. Hill, O. Jahn, P. Landschützer, J. M. Lauderdale, J. Liu, M. Manizza, J. D. Naviaux, C. Rödenbeck, D. S. Schimel, T. Van der Stocken, H. Zhang, The ECCO-Darwin Data-Assimilative Global Ocean Biogeochemistry Model: Estimates of seasonal to multidecadal surface ocean pCO_2 and air-sea CO_2 Flux. *J. Adv. Model. Earth Syst.* **12**, e2019MS001888 (2020).

30. R. C. Lewontin, D. Cohen, On population growth in a randomly varying environment. *Proc. Natl. Acad. Sci. U.S.A.* **62**, 1056–1060 (1969).

31. J. Roughgarden, A simple model for population dynamics in stochastic environments. *Am. Nat.* **109**, 713–736 (1975).

32. D. G. Heckel, J. Roughgarden, A species near its equilibrium size in a fluctuating environment can evolve a lower intrinsic rate of increase. *Proc. Natl. Acad. Sci. U.S.A.* **77**, 7497–7500 (1980).

33. C. Scott Baker, P. J. Clapham, Modelling the past and future of whales and whaling. *Trends Ecol. Evol.* **19**, 365–371 (2004).

34. V. J. D. Tulloch, É. E. Plagányi, C. Brown, A. J. Richardson, R. Matear, Future recovery of baleen whales is imperiled by climate change. *Glob. Change Biol.* **25**, 1263–1281 (2019).

35. M. S. Savoca, M. F. Czapanskiy, S. R. Kahane-Rapport, W. T. Gough, J. A. Fahlbusch, K. C. Bierlich, P. S. Segre, J. Di Clemente, G. S. Penry, D. N. Wiley, J. Calambokidis, D. P. Nowacek, D. W. Johnston, N. D. Pyenson, A. S. Friedlaender, E. L. Hazen, J. A. Goldbogen, Baleen whale prey consumption based on high-resolution foraging measurements. *Nature* **599**, 85–90 (2021).

36. O. Hoegh-Guldberg, J. F. Bruno, The impact of climate change on the world's marine ecosystems. *Science* **328**, 1523–1528 (2010).

37. G. C. Hays, A. J. Richardson, C. Robinson, Climate change and marine plankton. *Trends Ecol. Evol.* **20**, 337–344 (2005).

38. J. D. Stewart *et al*., stewart6/ENPGW-IPM: Data and Code for Stewart et al. Boom-bust cycles in gray whales. Zenodo (2023); https://doi.org/10.5281/zenodo.8201214.

39. J. L. Laake, A. E. Punt, Gray whale southbound migration surveys 1967–2006: An integrated re-analysis. *J. Cetacean Res. Manag.* **12**, 287–306 (2012).

40. J. W. Durban, D. W. Weller, A. R. Lang, W. L. Perryman, Estimating gray whale abundance from shore-based Counts using a multilevel Bayesian model. *J. Cetacean Res. Manag.* **15**, 61–68 (2015).

41. J. Laake, A. Punt, R. Hobbs, M. Ferguson, D. Rugh, J. Breiwick, “Re-analysis of Gray Whale 1967-2006,” NOAA Technical Memoradum NMFS-AFSC-203 (2009).

42. S. L. Swartz, M. L. Jones, Gray whale (*Eschrichtius robustus*) calf production and mortality in the winter range. *Rep. Int. Whaling Comm.* **34**, 503–507 (1983).

43. J. F. Samhouri, B. E. Feist, M. C. Fisher, O. Liu, S. M. Woodman, B. Abrahms, K. A. Forney, E. L. Hazen, D. Lawson, J. Redfern, L. E. Saez, Marine heatwave challenges solutions to human-wildlife conflict. *Proc. R. Soc. B Biol. Sci.* **288** (2021).

44. J. W. Durban, H. Fearnbach, A. Paredes, L. S. Hickmott, D. J. LeRoi, Size and body condition of sympatric killer whale ecotypes around the Antarctic Peninsula. *Mar. Ecol. Prog. Ser.* **677**, 209–217 (2021).

45. J. W. Durban, M. J. Moore, G. Chiang, L. S. Hickmott, A. Bocconcelli, G. Howes, P. A. Bahamonde, W. L. Perryman, D. J. LeRoi, Photogrammetry of blue whales with an unmanned hexacopter. *Mar. Mamm. Sci.* **32**, 1510–1515 (2016).

46. H. Fearnbach, J. W. Durban, L. G. Barrett-Lennard, D. K. Ellifrit, K. C. Balcomb III, Evaluating the power of photogrammetry for monitoring killer whale body condition. *Mar. Mamm. Sci.* **36**, 359–364 (2020).

47. F. Christiansen, S. Dawson, J. Durban, H. Fearnbach, C. Miller, L. Bejder, M. Uhart, M. Sironi, P. Corkeron, W. Rayment, E. Leunissen, E. Haria, R. Ward, H. Warick, I. Kerr, M. Lynn, H. Pettis, M. Moore, Population comparison of right whale body condition reveals poor state of the North Atlantic right whale. *Mar. Ecol. Prog. Ser.* **640**, 1–16 (2020).

48. F. Christiansen, A. M. Dujon, K. R. Sprogis, J. P. Y. Arnould, L. Bejder, Noninvasive unmanned aerial vehicle provides estimates of the energetic cost of reproduction in humpback whales. *Ecosphere* **7**, 1–18 (2016).

49. L. Soledade Lemos, J. D. Burnett, T. E. Chandler, J. L. Sumich, L. G. Torres, Intra- and inter-annual variation in gray whale body condition on a foraging ground. *Ecosphere* **11**, e03094 (2020).

50. F. Christiansen, F. Vivier, C. Charlton, R. Ward, A. Amerson, S. Burnell, L. Bejder, Maternal body size and condition determine calf growth rates in Southern right whales. *Mar. Ecol. Prog. Ser.* **592**, 267–281 (2018).

51. S. E. Moore, J. M. Grebmeier, J. R. Davies, Gray whale distribution relative to forage habitat in the northern Bering Sea: Current conditions and retrospective summary. *Can. J. Zool.* **81**, 734–742 (2003).

52. A. Gelman, A. Jakulin, M. G. Pittau, Y.-S. Su, A weakly informative default prior distribution for logistic and other regression models. *Ann. Appl. Stat.* **2**, 1360–1383 (2008).

53. R Core Team, R: A language and environment for statistical computing (R Foundation for Statistical Computing, 2021); http://www.r-project.org.

54. Stan Development Team, *Stan Modeling Language Users Guide and Reference Manual*, version 2.31 (2023); https://mc-stan.org.

55. A. Gelman, D. B. Rubin, Inference from iterative simulation using multiple sequences. *Stat. Sci.* **7**, 457–472 (1992).